

Rechargeable Lithium Metal Batteries with an In-Built Solid-State Polymer Electrolyte and a High Voltage/Loading Ni-Rich Layered Cathode

Chen-Zi Zhao, Qing Zhao, Xiaotun Liu, Jingxu Zheng, Sanjuna Stalin, Qiang Zhang, and Lynden A. Archer*

Solid-state batteries enabled by solid-state polymer electrolytes (SPEs) are under active consideration for their promise as cost-effective platforms that simultaneously support high-energy and safe electrochemical energy storage. The limited oxidative stability and poor interfacial charge transport in conventional polymer electrolytes are well known, but difficult challenges must be addressed if high-voltage intercalating cathodes are to be used in such batteries. Here, ether-based electrolytes are in situ polymerized by a ring-opening reaction in the presence of aluminum fluoride (AIF₃) to create SPEs inside LiNi_{0.6}Co_{0.2} Mn_{0.2}O₂ (NCM) || Li batteries that are able to overcome both challenges. AIF3 plays a dual role as a Lewis acid catalyst and for the building of fluoridized cathode-electrolyte interphases, protecting both the electrolyte and aluminum current collector from degradation reactions. The solid-state NCM || Li metal batteries exhibit enhanced specific capacity of 153 mAh g⁻¹ under high areal capacity of 3.0 mAh cm⁻². This work offers an important pathway toward solid-state polymer electrolytes for high-voltage solid-state batteries.

Solid-state electrolytes (SSEs) are emerging as the key solutions to meet the ever-growing energy storage demands for practical and long-lasting electrochemical energy storage in applications ranging from portable electronics to renewable energy sources. The improved safety features offered by SSEs relative to liquid electrolytes, particularly in electrical energy storage (EES) contexts where reactive alkali metals are used as anodes in

C.-Z. Zhao, Dr. Q. Zhao, X. Liu, S. Stalin, Prof. L. A. Archer Robert Frederick Smith School of Chemical and Biomolecular Engineering Cornell University

Ithaca, NY 14853, USA E-mail: laa25@cornell.edu C.-Z. Zhao, Prof. Q. Zhang

Beijing Key Laboratory of Green Chemical Reaction Engineering and Technology Department of Chemical Engineering

Tsinghua University Beijing 100084, China

J. Zheng

Department of Material Science and Engineering Cornell University

Ithaca, NY 14853, USA

The ORCID identification number(s) for the author(s) of this article can be found under https://doi.org/10.1002/adma.201905629.

DOI: 10.1002/adma.201905629

high-energy-density rechargeable batteries, are among the most important motivations for interest in SSEs. Moreover, other factors such as constructing batteries where leakage or vaporization of a liquid electrolyte can be avoided or in which battery cells can be easily integrated into wearables are also major opportunity areas for SSEs.^[1] Additionally, when mS cm⁻¹ level room temperature ionic conductivity is achieved, SSEs offer promising opportunities to fully utilize the ultrahigh energy storage ability enabled by high-voltage intercalation and alkali metal chemistry.^[2]

SSEs of contemporary interest generally fall into two categories: inorganic ceramic electrolytes and solid-state polymer electrolytes (SPEs). Inorganic materials including oxides and sulfides are investigated because they possess high ambient temperature ionic conductivities, even surpassing those of their liquid electrolyte counterparts

in some cases.^[3,4] However, the intrinsic rigidity, brittleness, and environmental sensitivity continue to pose significant challenges to the development of practical cells based on such materials. Furthermore, battery cells based on poorly conductive active materials require intimate/conformal contact between the electrolyte and electrode to achieve short-enough transportation distances in the electrode to ensure complete active material utilization.^[5] As a result practical solid-state batteries based on state-of-the-art intercalating transition metal oxide cathodes are not yet available.

Organic-polymer-based SSEs take advantage of the light weight, low cost, mechanical toughness, and low/non-volatility; furthermore, the manufacturability of synthetic polymers offers intrinsic mechanisms for overcoming many of the limitations of solid-state inorganic electrolytes. As a result, they are receiving intensive interest.^[6-10] However, multiple difficult challenges remain including the large thermodynamic driving force for macromolecular stacking and crystallization, which generally yields low ambient-temperature ionic conductivity; and the difficulty in infiltrating the highly viscous molten polymers into the nano-sized pores of intercalating cathodes, especially when high-loading materials are utilized for enhanced energy density. [11–15] Furthermore, the most widely studied polymer electrolytes such as poly(ethylene oxide) (PEO) that afford acceptable conductivity and are compatible with

alkali metal anodes, have limited oxidative stability at stateof-the-art nickel-rich transition metal cathodes, which limits their utility.[16-23] Besides, polymer electrolytes require highconcentration Li salts composed of large anions, most notably lithium bis(trifluoromethanesulfonyl)imide (LiTFSI) or lithium bis(fluorosulfonyl) imide (LiFSI), to achieve sufficient amounts of dissociated ion pairs for efficient ion transport at room temperature. [6,24,25] Unfortunately, these salts are known for their propensity of severe current collector corrosion through both chemical and electrochemical reactions during battery cycling,[26-28] which creates a risk of orphaned active materials and abrupt capacity drop. To mitigate these problems, high-voltage stable molecules such as carbonates are generally introduced.^[29] Artificial cathode-electrolyte interphases (CEI) produced by coating the active cathode materials with desirable compounds such as organophosphates,^[30] polypyrrole (PPy),^[31] phosphate polyanion,^[32] Al₂O₃,^[33] and NaTi₂(PO₄)₃^[34] have also been reported to protect the cathode. However, the most successful coating strategies are demonstrated in carbonate-based liquid electrolytes, which introduce new stability challenges when the cathodes are paired with high-energy alkali metal

Herein, we investigate solid-state batteries created by in-situ polymerization of liquid electrolytes inside a battery cell. By taking advantage of the low viscosity and interfacial interactions of the liquid precursors, [35–37] such electrolytes are reported to overcome conventional problems with poor interfacial charge

transport. SSEs based on polymerized 1,3-dioxolane (Poly-DOL) are of particular interest because this polymer forms chemically stable interphases on Li metal and thereby enables highly reversible cycling of Li metal anodes.[38] Ring-opening polymerization of DOL in the presence of a mixture of Lewis acids, AlF₃, and aluminum triflate (Al(OTf)₃) is shown herein, further, to provide a general approach for creating poly-DOL SSEs with in-built functionality to stabilizing the electrolyte at the reducing potentials of a Li metal anode and the oxidizing potentials of a LiNi_{0.6}Co_{0.2}Mn_{0.2}O₂ (NCM622) cathode. The AlF₃ and Al(OTf)3 are introduced as salt additives in the liquid electrolyte precursor to facilitate complete wetting of the porous NCM cathode and Li anode. The polymerization reaction is gradual and results in formation of a solid-state polymer with well-formed interphases at both the cathode and anode that provide in-built connected pathways for ion migration. The AlF₃ also appears to play a dual role in CEI construction and current collector protection, facilitating electrolyte stability, and thus practical cycling performances of NCM622 || Li cells.

Ring-opening polymerization of DOL was initiated by a mixture of Al(OTf)₃ and AlF₃, with 2.0 $\,\mathrm{m}$ LiTFSI introduced in the electrolyte. The reaction was carried out at 25 °C and monitored by small-amplitude oscillatory shear rheology at a shear strain $\gamma = 0.5\%$ for an extended period of time (**Figure 1**a; Figure S1, Supporting Information). The polymerization reaction produced a large increase in both the elastic/storage modulus (G') and viscous/loss modulus (G'') of the materials; completion of

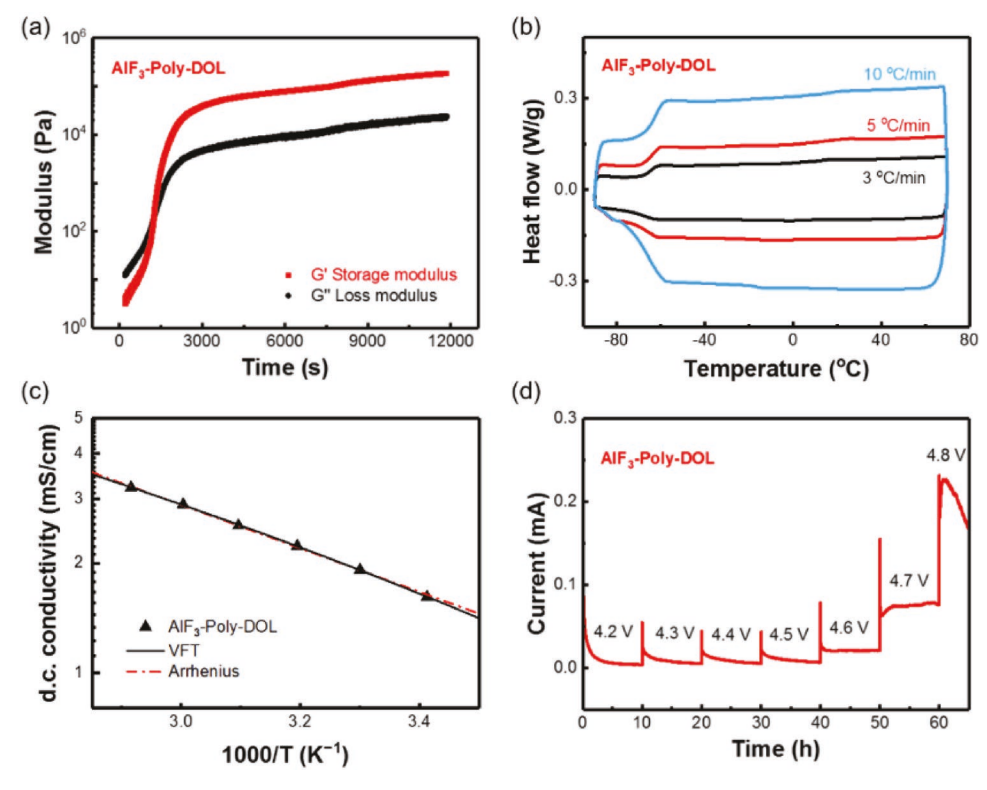


Figure 1. Characteristics of AlF₃-Poly-DOL electrolyte. a) Time sweep rheology measurements for AlF₃-Poly-DOL electrolyte at angular frequency $\omega = 10$ rad s⁻¹. The material has a higher storage modulus G' and is thus more solid-like after polymerization process. b) DSC analysis of AlF₃-Poly-DOL electrolyte. c) Conductivity of the AlF₃-Poly-DOL electrolytes versus temperature (0.3 \upmu AlF₃). The solid (black) and dashed (red) lines through the data are fitted using the Vogel–Fulcher–Tammann (VFT) and Arrhenius transport models, respectively. d) Electrochemical floating analysis of the AlF₃-Poly-DOL electrolyte using NCM cathodes.

the reaction was identified by the plateauing of both moduli. During the earliest stages of polymerization, the electrolyte is liquid-like and G''>> G'. As the polymer chains grow and begin to entangle, G' increases more quickly with time, eventually becoming larger than G''. By the end of the polymerization process the electrolyte is transformed to a solid-state, elastic material for which $G' \approx 10G''$, and the elastic modulus of the resultant SSE approaches values typical of polyether melts.^[39] Upon completion of the polymerization, the weight average molecular weight ($M_{\rm w}$) of the AlF₃-Poly-DOL (0.3 M AlF₃) electrolyte reached 18 kDa with dispersity Φ of 1.59 as measured by gel permeation chromatography (GPC) in tetrahydrofuran. In addition, the molecular weights decrease with the increase of AlF₃ concentration (Table S1, Supporting Information).

The thermal properties of the in situ formed poly-DOL were measured by differential scanning calorimetry (DSC) at different scan rates. (Figure 1b) The material was first heated above its melting transition to eliminate any thermal history. The poly-DOL also exhibited a low glass transition temperature ($T_{\rm g}$) of around –70 °C, which implies that under ambient conditions accelerated segmental motions occur, leading to superior ion transport properties at room temperature.

Ionic transport properties of the in situ polymerized AlF₃-Poly-DOL electrolyte are shown in Figure 1c. The poly-DOL electrolytes exhibit ionic conductivities at mS cm⁻¹ level at both room and elevated temperatures, where the conductivities are enhanced with the addition of AlF3 additives compared with routine Poly-DOL electrolyte.[38] The enhancement is thought to originate from the decrease in the average poly-DOL molecular weight, because AlF₃ is itself a strong Lewis acid capable of initiating ring-opening polymerization of DOL (Figure S2, Supporting Information). At the lower polymer molecular weights studied here, both features lower the glass transition temperature, which facilitates ion migration. The X-ray diffraction (XRD) patterns indicate that no obvious crystallinity is observed for the SPE (Figure S3, Supporting Information). The temperature-dependent conductivity for the in situ polymerized electrolyte can be fitted well either using the Arrhenius or Vogel-Fulcher-Tammann equation (Table S2, Supporting Information). This finding is consistent with the low T_{o} of the materials and reflects the fact that the conductivity data in Figure 1c are measured at temperatures well above the glass transition temperature of the electrolyte. It should be noted that in most cases a small fraction of incompletely polymerized liquid-like DOL remains in the SPE plays a role in the favorable bulk and interfacial transport properties (Figure S4, Supporting Information).

A well-known, but stubborn problem faced by all ether-based electrolytes is their poor oxidative stability at the battery cathode, where modifying Li salts contributes to extending the electrochemical stability window of ether-based liquid electrolytes. [40] Quantifying the leakage current measured in an electrochemical floating test provides an aggressive approach for evaluating this stability. Results reported in Figure 1d indicate that AlF₃-Poly-DOL electrolyte exhibits limited leakage current as high as 4.7 V. A more rigorous approach for characterizing stability of a polymer SSE is to evaluate the performance of rechargeable batteries composed of Ni-rich nickel-cobalt-manganese oxides cathodes. Here, we investigated

the reversibility of NCM622 \parallel Li metal batteries composed of commercial cathodes with a high areal loading of 3.0 mAh cm⁻² and utilizing the in situ formed poly-DOL SSEs (Figure 2). The results reported in Figure 2a show that the AlF₃-Poly-DOL batteries are able to operate without overcharging or side reactions at an elevated cut-off voltage of 4.2 V, which is consistent with the floating test results showing excellent anodic stability. However, there is a continuous capacity decay and a sudden drop after the 20th cycle for routine Poly-DOL electrolytes. We hypothesize that this behavior reflects the limited compatibility of the Poly-DOL electrolyte with the NCM cathode.

We compared cycling performance of the NCM622|poly-DOL|Li cells with those of analogous batteries in which AlF₃ is present at various concentrations in the electrolytes. Defining the cycle life as the number of complete charge/discharge cycles that the batteries support before the capacity falls under 80% of its original capacity, results reported in Figure 2b show that the cycle life of the NCM || Li metal batteries exhibit a bellshaped dependence on AlF3 concentration. The results show that poly-DOL electrolytes containing 0.3 M AlF₃ produce the largest enhancement in cycle life, exhibiting specific capacity of 153 mAh g⁻¹ and extended stability (Figure S5, Supporting Information). At elevated current density of 0.5 C, the NCM || Li metal battery remain over 80% capacity over 30 cycles (Figure S6, Supporting Information). The cells containing this electrolyte also exhibit favorable charge/discharge rate capabilities and good capacity recovery (Figure S7, Supporting Information). The average Coulombic efficiency of lithium metal anode is 92.9% under 1.0 mAh cm⁻² at current density of 1.0 mA cm⁻² for first ten cycles (Figure S8, Supporting Information).

To understand the reasons for the improved cycling stability, a postmortem investigation was carried out to study NCM cathode material's evolution before and after continuous cycling. Before cycling, the NCM active material together with conductive carbon and binder is uniformly coated on Al foil (Figure 3a,d), the current collector. After cycling in the AlF₃-Poly-DOL electrolytes, the in situ polymerization process evidently enables the polymer electrolytes to fill the pores of the NCM to form good CEI on the active particles (Figure 3b). Notably, the postmortem investigations reveal that the Al current collector for the NCM cathode is severely corroded in some cases (low AlF₃ concentrations in the electrolyte), where the current collector disappears entirely after continuous cycling (Figure 3c). The cross-section view illustrates the corrosion phenomenon most clearly. There is a clear boundary between the Al foil and NCM active layer for the pristine NCM cathode, indicating that the Al current collector has a thickness of ≈30 µm and the high-loading NCM layer is 60 µm thick (Figure 3d). After cycling, the current collector is intact, with little or no reduction in thickness for AlF3-Poly-DOL electrolytes (Figure 3e). In comparison, the current collector is obviously eroded in Poly-DOL electrolytes without AlF₃ (Figure 3f; Figure S9, Supporting Information). The corrosion is itself complex. The thick NCM layer invades the Al current collector and the Al foil is dissolved leaving holes and scraps. Energydispersive X-ray spectroscopy (EDS) mapping of the electrode (Figure 3f) reveals aluminum fragments accumulate on top of the NCM layer, indicating that the Al current collector is partially broken during cycling.

www.advancedsciencenews.com

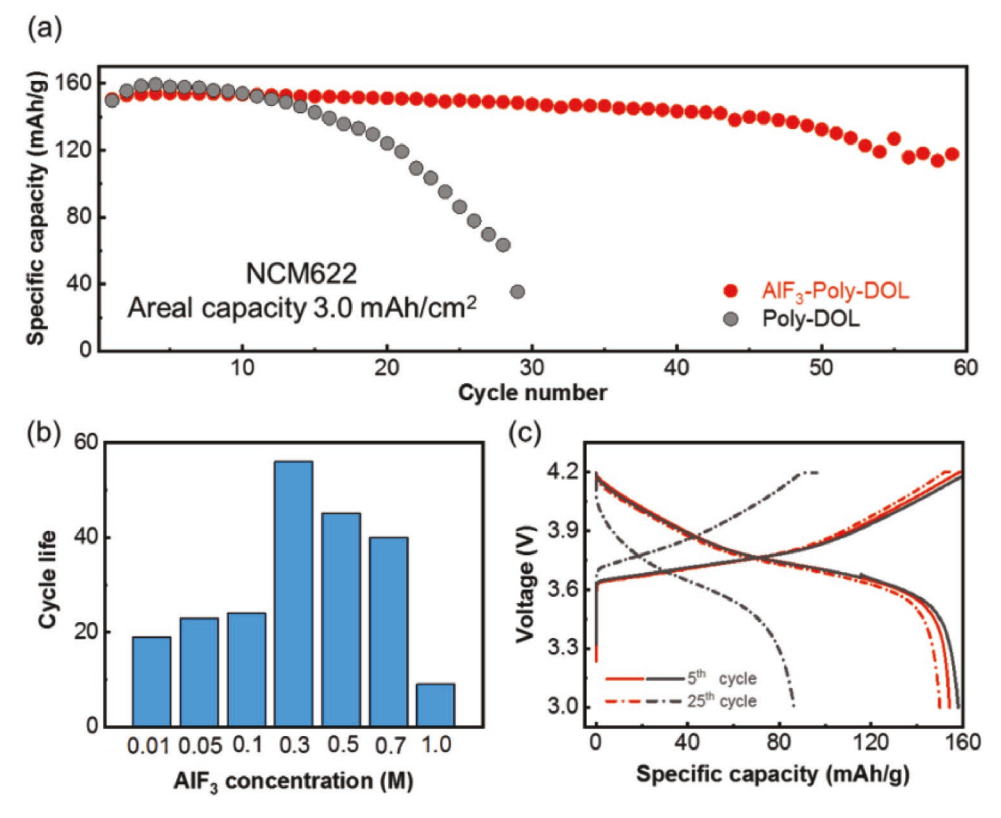


Figure 2. Electrochemical performances of cells using high-loading NCM cathodes and Li metal anodes. a) Galvanostatic cycling performances of solid-state NCM \parallel Li metal batteries with AlF₃-Poly-DOL and routine polymerized DOL at 0.1 C under room temperature. b) Cycle life of high-loading NCM batteries with different AlF₃ concentrations in poly-DOL electrolytes. c) Corresponding discharge/charge profiles of NCM batteries with 0.3 $\,$ M AlF₃-Poly-DOL (red) and Poly-DOL (gray) electrolytes.

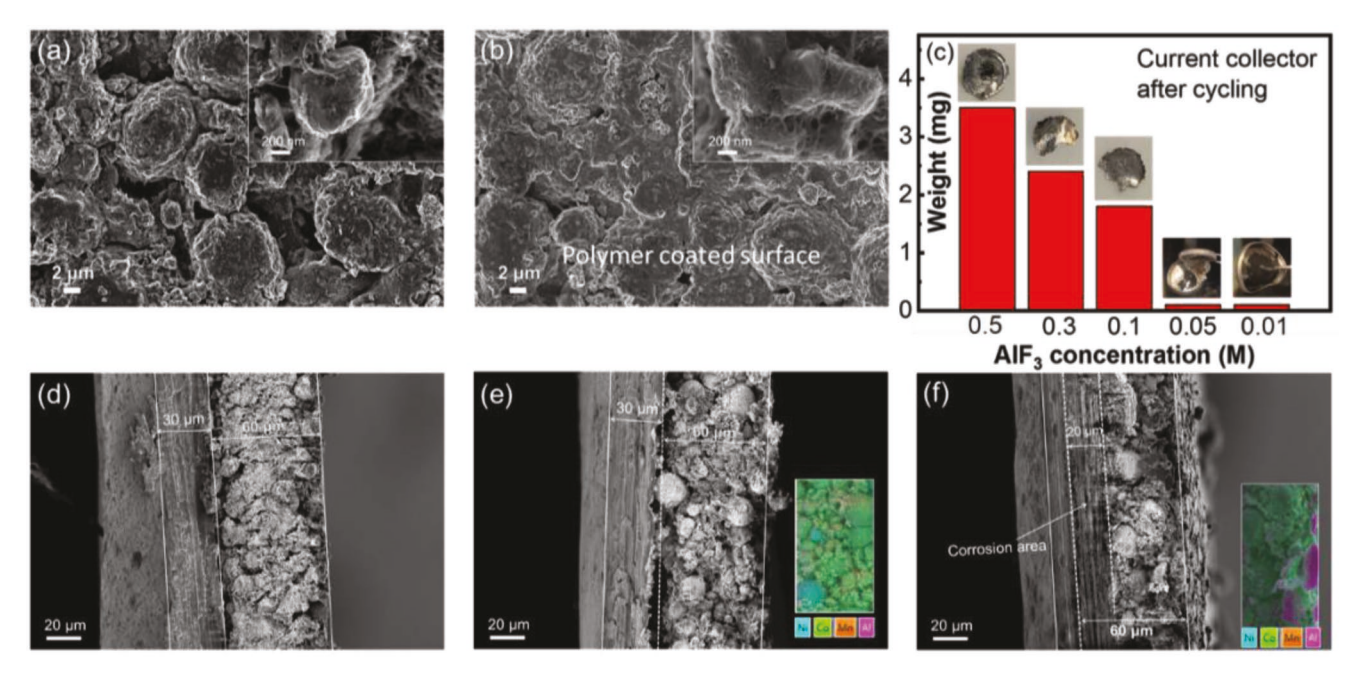
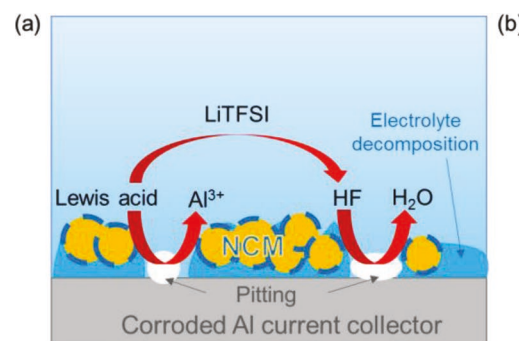
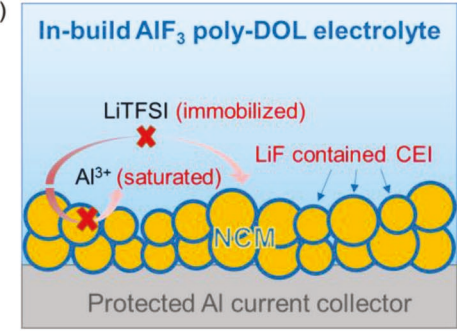


Figure 3. Morphologies of NCM cathode before and after cycling. a,b) Scanning electron microscopy (SEM) images of the NCM cathode surface before (a) and after (b) cycling in 0.3 M AIF₃-Poly-DOL electrolytes. Insert is the enlarged images of NCM particles. c) Morphologies and the weight of cathode current collectors after continuous cycling in poly-DOL electrolyte with different AIF₃ concentrations. d–f) Cross section view of NCM cathode before cycling (d), after cycling in routine Poly-DOL electrolytes (e), and after cycling in AIF₃-Poly-DOL electrolytes (f). Inset is the energy-dispersive X-ray spectroscopy (EDS) mapping of Ni, Co, Mn, Al element for the NCM layer after cycling.





Scheme 1. a,b) Schematic diagrams of current collector corrosion in routine electrolytes (a) and AIF₃-Poly-DOL electrolytes (b).

The dissolution potential of Al is complicated because the corrosion reaction is sluggish and involves lots of related reactions, such as TFSI anion decomposition and solvent oxidation. [28,41] To identify the main Al corrosion reactions, Al || Li metal cells utilizing Al foil as the working electrode were created and their electrochemical behaviors were investigated in detail. Liquid electrolytes composed of mixtures of ethylene carbonate/dimethyl carbonate (EC/DMC) solvents were used in these experiments to remove contributions from ether electrolyte decomposition at elevated voltages. Results from electrochemical floating experiments (Figure S10, Supporting Information) reveal an increased leakage current at approximately 4.3 V versus Li metal, suggesting that a severe reaction occurs at around 4.3 V. Linear sweep voltammetry (LSV) analysis of the Al || Li cells at a low scan rate of 0.02 mV s⁻¹ reveals a peak between 4.0 and 4.4 V, before an exponential increase is apparent (Figure S11a,b, Supporting Information). As carbonate-based electrolytes are known to be stable in this voltage range, it is speculated that the current peak is related to the oxidation reactions on aluminum working electrodes, which is consistent with reported results. [26,41,42] This perspective is supported by results from the analogous experiments using AlF₃-Poly-DOL electrolytes, where the leakage current around the oxidation peak is fairly limited (Figure S11c,d, Supporting Information).

To understand the role of AlF₃, we performed currentvoltage (CV) experiments (Figure S12, Supporting Information) on the Al | Li cells within a similar voltage range as for the NCM || Li metal batteries to imitate the electrochemical environment experienced by the Al current collector during cycling of these cells. The concentration of lithium salts is kept constant to facilitate systematic comparisons. It is believed that the Al electrode is passivated during the first scan, and in the following scan Al is continuously oxidized and dissolved in the electrolyte. [27,40] Batteries utilizing the liquid DOL electrolytes show the most severe evidence of degradation reactions (Figure S12a, Supporting Information). Polymerization of the DOL reduces the parasitic reactions and improve electrochemical stability (Figure S12b, Supporting Information). Further, adding AlF3 to the Poly-DOL electrolytes visibly decrease the degradation currents (Figure S12c, Supporting Information). Since the ionic conductivities of the electrolytes are of the same order of magnitude, the much-reduced leakage current is thought to be the result of a passivation layer formed on the aluminum foil. We hypothesize further that multiple reactions

are likely responsible for the Al corrosion (**Scheme 1**). In particular, the Lewis acids present in the electrolytes generate protons from slow electrochemical oxidation at the cathodes, which we believe are responsible for breaking down the Al₂O₃ layer on Al foil to produce soluble Al³⁺ species. The protons can also react with LiTFSI salt in electrolytes to generate HF, which may further etch the Al current collector. [28,43] Introducing AlF₃ additives in poly-DOL electrolytes is thought to create a solution saturated with Al³⁺ and immobilize TFSI⁻, which would inhibit Al₂O₃ dissolution.

The components of CEI are now understood to be crucial in stabilizing the cycling performances of nickel-rich, high-voltage cathodes such as NCM. X-ray photoelectron microscopy (XPS) analysis and EDS were used to probe the chemical features of NCM surface. The C 1s spectra (Figure 4a,e) indicate that common carbonaceous species, such as C-C, C-O, and C-F from conductive carbon or the polyvinylidene fluoride (PVDF) binder, are present on both electrodes. There is a unique protuberance of O-C=O peak on NCM cathodes cycled in the neat (no AlF₃) Poly-DOL electrolytes, which can be related to poly-DOL high-voltage decomposition in the absence of AlF₃. The aluminum peaks in Figure 4c indicate the peeling of the Al foil due to Al corrosion after cycling in the neat Poly-DOL, which is barely detected on cathodes cycled in AlF3-Poly-DOL electrolytes (Figure 4g) and consistent with results from the EDS mapping reported in Figure 3. Moreover, due to the limited detection depth of XPS surface analysis, the identification of obvious Ni peaks suggests the exposure of active NCM material, while the NCM particles are tightly coated by polymer layer contacting AlF₃-Poly-DOL electrolytes (Figure 4d,h).

Analysis of the F 1s spectra indicates additional AlF₃ contributes to the generation of LiF in the CEI layer (Figure 4b,f). EDS results confirm the introduction of fluoride on NCM cathode after cycling in AlF₃-Poly-DOL electrolytes (Figure S13 and Table S3, Supporting Information). Lithium fluoride is known for its ability to protect Li metal anodes and its presence at interphases formed in solvent-in-salt type electrolytes has been speculated to enhance oxidative stability of electrolyte solvents. [44–47] To explore these effects in greater detail, LiF salts were directly introduced as additives in the DOL precursor and polymerized in situ in the NCM622 \parallel Li cells. The galvanostatic cycling properties of these cells are reported in Figure S14, Supporting Information. The results show that an extended cycle life is achieved, demonstrating that directly adding LiF can enhance cycling stability. However, a sudden capacity drop after

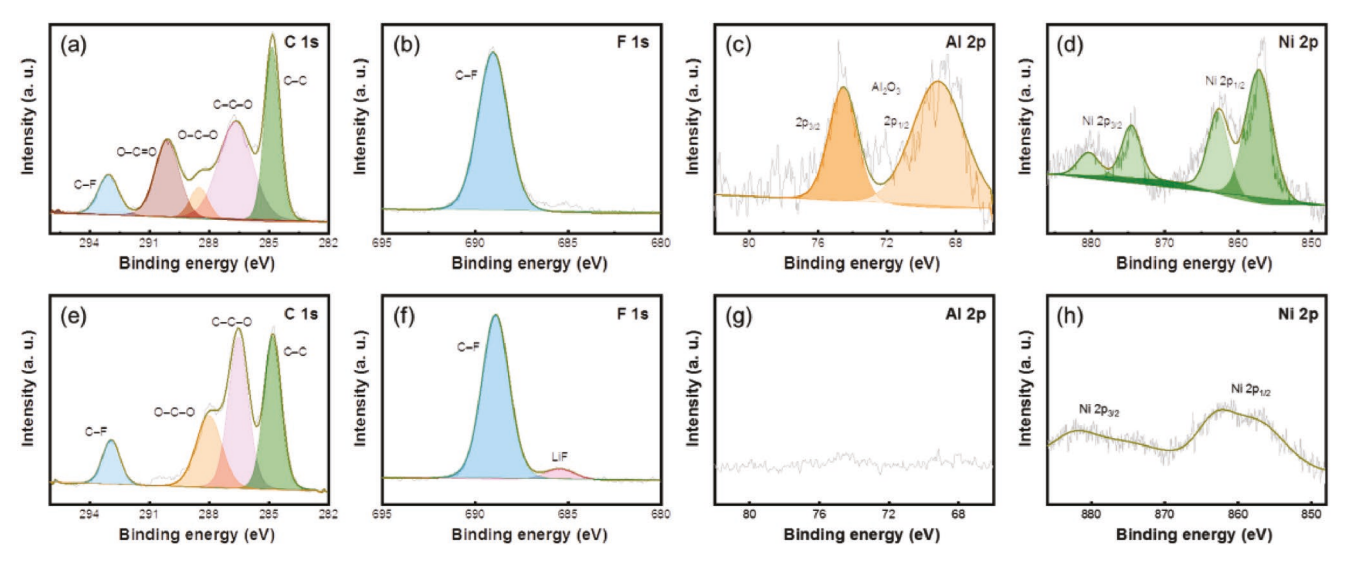


Figure 4. Surface analysis of NCM cathode after cycling. a–h) XPS spectra of NCM cathode after cycling in routine Poly-DOL electrolyte (a–d) and AIF₃-Poly-DOL electrolyte (e–h).

30 cycles is still observed probably due to the current collector corrosion or an in-complete protective layer formed by the LiF salt additive.

Although AlF3 particles in poly-DOL electrolytes are beneficial for current collector protection and CEI construction, excess amount of AlF3 results in decreased ionic conductivity (Figure S15 and Table S2, Supporting Information) and significantly increased impedance both before and after cycling (Figure S16, Supporting Information), as AlF₃ itself exhibits a wide bandgap (>10 eV) and is almost an ionic insulator. Consequently, there is a trade-off between cathode protection and ion transportation ability. The cycle life of the NCM622|AlF3-Polv-DOLILi solid-state batteries is nonetheless not vet at levels required for practical implementation. The gradual capacity fading observed in Figure 2a, particularly after cycle 50, is attributed not only necessarily to the AlF₃-Poly-DOL electrolyte, but to other failure modes, including cathode phase transition, increased internal resistances, or Li metal consumption. Among these, the failure modes of changes in NCM structure have been reported previously as a prominent phenomenon after charge-discharge cycling at potentials in the range used in the study. [40,48,49] XRD was used to analyze lattice distortion of LiNi_{0.6}Co_{0.2}Mn_{0.2}O₂ (Figure S17, Supporting Information). The presence of extra nickel ions in Li inter-slab space, primarily owing to the similar radius of Ni²⁺ (0.69 Å) and Li⁺ (0.76 Å), makes it difficult for lithium ions to intercalate into the structure during cell discharge.^[50-52] This cation disorder leads to changes in c/a axis and layered structure, which is verified through the decreased intensity ratio of plane (003) (104) and the split of plane (108) (110) in XRD spectra. Although $I_{(003)}/I_{(104)}$ for the NCM cathodes is lowered for both electrolytes (Figure S17b, Supporting Information), the introduction of AlF₃ inhibits the cation disorder. Al³⁺ in the transition layer increases the c axis parameter and reduces the a axis parameter, due to the shortened a-axis but extended c-axis parameters of α-LiAlO₂ compared with LiNiO₂, thus contributing to the stabilization of the crystal structure.^[53–55] However, the position separation of (110) and (018) plane after cycling indicates the distortion of layered structure (Figure S17c, Supporting Information), which is also responsible for the capacity decay.^[48]

Our finding that AlF₃ electrolyte salt additives improve cycling of NCM cathodes in poly-DOL electrolytes can be extended to other electrolyte systems for enhanced stability and compatibility with high-voltage cathodes. Results reported in Figure S18, Supporting Information, show that addition of AlF₃ to carbonate electrolytes prevents the sudden capacity fade (in this case at cycle 55) typically observed.^[56] An even more obvious benefit of AlF₃ is apparent in Figure S19, Supporting Information, where it is used as an additive in solid-state secondary batteries composed of poly(ethylene oxide) (PEO) electrolytes. PEO-based electrolytes are notorious for their extremely poor oxidative stability and cannot be cycled in an electrolyte without AlF₃. Our results show that AlF₃ improves the electrochemical stability of PEO, to at least 4.3 V, and facilitates cycling of NCM cathodes.

In summary, we propose an in situ formed solid-state polymer electrolyte using ether-based liquid precursors and Lewis acid salts that initiate ring-opening polymerization. The addition of AlF_3 to the electrolytes is shown to enhance their anodic stability. The in-built solid ionic conductors are compatible with high-loading NCM cathodes, and the principal role of the AlF_3 salt is demonstrated to be in passivating the current collector surface under high-voltage conditions, where AlF_3 dissolution reaction is suppressed. AlF_3 also contributes other beneficial effects, including creation of high-quality CEI layer, resulting in extended cycle life of NCM \parallel Li metal batteries in poly-DOL, carbonates, and PEO-based electrolytes.

Experimental Section

Electrolyte Preparation: The AlF $_3$ -Poly-DOL electrolyte mentioned herein represents 0.3 M AlF $_3$ -Poly-DOL electrolytes with 0.5 mM Al(OTf) $_3$ and 2 M LiTFSI unless otherwise specified. AlF $_3$ was partially soluble in DOL electrolyte; undissolved AlF $_3$ particles were clearly observed in the dispersion at concentrations higher than 0.1 M.

www.advancedsciencenews.com

www.advmat.de

Electrolytes used in the study were prepared in an argon-filled glove box. AlF₃ (Alfa Aesar), LiTFSI (Alfa Aesar; TCI America), and Al(OTf)₃ (Alfa Aesar) were used without further purification AIF₃ was milled before use. DOL (Sigma-Aldrich) was treated for at least 1 day with fresh Li metal to remove any traces of water remaining in the electrolytes. Polymerization was conducted by preparing 5 mm Al(OTf)₃ DOL solution first, then diluting the solution to 0.5 mm Al(OTf)₃ DOL with the DOL-LiTFSI-AlF₃ electrolyte. The DOL-LiTFSI-AlF₃ diluent was prepared by adding AlF₃ and 2 M LiTFSI salt to DOL solution successively. For free-standing PEO electrolytes, PEO 600K (Sigma-Aldrich) was employed. Halloysite nanoclay (HNC, Sigma Aldrich), AlF3 (Alfa Aesar), LiTFSI (Alfa Aesar; TCI America), and LiNO₃ (Sigma-Aldrich) were used to improve mechanical properties and suppress PEO crystallinity. The EO/LiTFSI mole ratio was maintained at 10. The mass ratios of LiNO₃ and AlF₃ were both 10%. PEO, HNC, AIF3, LiTFSI, and LiNO3 were mixed in acetonitrile (Sigma-Aldrich) to form a homogeneous slurry. The slurry was casted into a polytetrafluoroethylene (PTFE) mold.

Battery Assembly and Test: Batteries were assembled in an argon glove box. The NCM cathodes were commercial and with areal capacity loading of 3.0 mAh $\,\mathrm{cm^{-2}}$. Both punched NCM cathodes and Li metal anodes were stored in the glove box. Coin 2032-type cells were used. The cells were assembled by adding 5 mm Al(OTf)₃ DOL to cathode side first, then DOL-LiTFSI-AlF₃ diluent electrolytes to obtain a poly-DOL electrolyte with 0.5 mm Al(OTf)3, 2 m LiTFSI, and AlF3 particles. DOL-LiTFSI-AlF₃ electrolytes were added on both sides of Celgard 3501 separator for a uniform AIF₃ dispersion. The DOL-LiTFSI-AIF₃ electrolytes were mixed well before battery assembly. The Celgard separator was used to avoid short circuit in the liquid state. All the batteries with poly-DOL electrolytes were tested after polymerization process. Galvanostatic discharge-charge tests were performed using a Neware battery tester at room temperature. NCM batteries with poly-DOL electrolytes were charge-discharged within 3.0-4.2 V at 0.1 C. NCM || Li metal batteries utilizing EC/DMC electrolytes were assembled with/without 0.1 M AIF3 in 2 $\,\mathrm{M}$ LiTFSI EC/DMC (v/v 1:1) electrolytes. The added AlF $_3$ was also partially soluble in EC/DMC electrolytes. Electrolytes were also added on both sides of Celgard 3501 separator for a uniform AIF₃ dispersion. NCM batteries with EC/DMC electrolytes were charge-discharged within 3.0-4.2 V at 0.2 C, where the first formation cycle was operated at 0.1 C. Batteries with PEO electrolytes were assembled with free-standing PEO electrolytes and no other separators were employed. The cathode utilized for PEO-based electrolytes is $\rm LiNi_{1/3}Co_{1/3}Mn_{1/3}O_2$ (NCM111), and the active material loading was around 2–3 mg cm $^{-2}$. Assembled batteries were pretreated at 80 °C overnight and tested at 60 °C. NCM batteries with PEO electrolytes were charge-discharged within 3.0-4.2 V at 0.1 C. The Coulombic efficiency (CE) of Li metal anodes was measured in Li || Cu cells.^[57] First, a certain amount of lithium (5.0 mAh cm⁻²) was plated and stripped as a "stabilization process" to form a passivation layer on electrodes. Then, a given amount of lithium (Q_T, 5.0 mAh cm⁻², 1.0 mA cm⁻²) was first deposited on Cu substrate as Li reservoir. Afterward, a smaller amount of this charge (Q_C, 1.0 mAh cm⁻², 1.0 mA cm⁻²) was plated and stripped for n (n = 10) cycles. Finally, the remaining Li reservoir (Q_S) were stripped until the cut-off voltage of 1.0 V. The average CE was calculated based on

$$CE_{avg} = \frac{nQ_C + Q_S}{nQ_C + Q_T} \tag{1}$$

A CH 600E electrochemical workstation was used for the cyclic voltammetry measurements. The electrochemical floating experiments were conducted in NCM || Li metal cells, which were charged to 4.2 V first, then held at progressively higher voltages, each for a period of 10 h.

Material Characterizations: Oscillatory shear rheology was conducted with a strain-controlled ARES-LS rheometer (Rheometric Scientific) outfitted with cone and plate geometry (4° cone angle, 10 mm diameter) for monitoring the polymerization reaction. DSC test was performed utilizing a Q1000 modulated differential scanning calorimeter (TA Instruments). GPC measurements were conducted by first dissolving the synthesized poly-DOL electrolytes in tetrahydrofuran (THF), then

eluting it in a Waters ambient temperature GPC. Polystyrene standards were used for the calibration. For NMR analysis, the electrolytes were dissolved in dimethyl sulfoxide-d $_6$. SEM images were obtained using a Gemini 500 field-emission scanning electron microscope equipped with energy-dispersive spectroscopy. XRD tests were conducted on a Bruker D8 Discover powder diffractometer using Cu K α radiation with a wavelength of approximately $\lambda = 1.54$ Å.

Supporting Information

Supporting Information is available from the Wiley Online Library or from the author.

Acknowledgements

C.-Z.Z., Q.Z. and X.L. contributed equally to this work. The work was supported by the Department of Energy Basic Energy Sciences Program through Award DE-SC0016082. Q.Z. is grateful to the Beijing Institute of Collaboratory Innovation (BICI) for financial support. Electron microscopy, XRD and XPS analysis were performed in facilities supported by the Cornell Center for Materials Research with funding from the NSF MRSEC program (DMR-1719875).

Conflict of Interest

The authors declare no conflict of interest.

Keywords

current collectors, high-voltage systems, in situ polymerization, Li-metal batteries, solid-state polymer electrolytes

Received: August 29, 2019 Revised: December 21, 2019 Published online:

- J. Lopez, D. G. Mackanic, Y. Cui, Z. Bao, Nat. Rev. Mater. 2019, 4, 312.
- [2] M. Armand, J. M. Tarascon, Nature 2008, 451, 652.
- [3] D. Aurbach, B. Markovsky, G. Salitra, E. Markevich, Y. Talyossef, M. Koltypin, L. Nazar, B. Ellis, D. Kovacheva, J. Power Sources 2007, 165, 491.
- [4] F. Lu, Y. Pang, M. Zhu, F. Han, J. Yang, F. Fang, D. Sun, S. Zheng, C. Wang, Adv. Funct. Mater. 2019, 29, 1809219.
- [5] J. C. Bachman, S. Muy, A. Grimaud, H.-H. Chang, N. Pour, S. F. Lux, O. Paschos, F. Maglia, S. Lupart, P. Lamp, L. Giordano, Y. Shao-Horn, Chem. Rev. 2016, 116, 140.
- [6] D. Lin, P. Y. Yuen, Y. Liu, W. Liu, N. Liu, R. H. Dauskardt, Y. Cui, Adv. Mater. 2018, 30, 1802661.
- [7] J. Li, C. Ma, M. Chi, C. Liang, N. J. Dudney, Adv. Energy Mater. 2015, 5, 1401408.
- [8] Q. Lu, Y.-B. He, Q. Yu, B. Li, Y. V. Kaneti, Y. Yao, F. Kang, Q.-H. Yang, Adv. Mater. 2017, 29, 1604460.
- [9] J.-Y. Liang, X.-X. Zeng, X.-D. Zhang, P.-F. Wang, J.-Y. Ma, Y.-X. Yin, X.-W. Wu, Y.-G. Guo, L.-J. Wan, J. Am. Chem. Soc. 2018, 140, 6767.
- [10] W. Huang, Z. Zhu, L. Wang, S. Wang, H. Li, Z. Tao, J. Shi, L. Guan, J. Chen, Angew. Chem., Int. Ed. 2013, 52, 9162.
- [11] W. Zhou, Z. Wang, Y. Pu, Y. Li, S. Xin, X. Li, J. Chen, J. B. Goodenough, Adv. Mater. 2019, 31, 1805574.

- [12] A. Du, H. Zhang, Z. Zhang, J. Zhao, Z. Cui, Y. Zhao, S. Dong, L. Wang, X. Zhou, G. Cui, Adv. Mater. 2019, 31, 1805930.
- [13] J. Bae, Y. Li, J. Zhang, X. Zhou, F. Zhao, Y. Shi, J. B. Goodenough, G. Yu, Angew. Chem., Int. Ed. 2018, 57, 2096.
- [14] R. Xu, Y. Xiao, R. Zhang, X.-B. Cheng, C.-Z. Zhao, X.-Q. Zhang, C. Yan, Q. Zhang, J.-Q. Huang, Adv. Mater. 2019, 31, 1808392.
- [15] H. Duan, M. Fan, W.-P. Chen, J.-Y. Li, P.-F. Wang, W.-P. Wang, J.-L. Shi, Y.-X. Yin, L.-J. Wan, Y.-G. Guo, Adv. Mater. 2019, 31, 1807789.
- [16] J. W. Choi, D. Aurbach, Nat. Rev. Mater. 2016, 1, 16013.
- [17] J. Mindemark, L. Imholt, J. Montero, D. Brandell, 2016, 54, 2128.
- [18] M. S. Whittingham, Chem. Rev. 2014, 114, 11414.
- [19] M. D. Tikekar, S. Choudhury, Z. Tu, L. A. Archer, Nat. Energy 2016, 1, 16114.
- [20] D. Lin, Y. Liu, Y. Cui, Nat. Nanotechnol. 2017, 12, 194.
- [21] Y. Liang, C.-Z. Zhao, H. Yuan, Y. Chen, W. Zhang, J.-Q. Huang, D. Yu, Y. Liu, M.-M. Titirici, Y.-L. Chueh, H. Yu, Q. Zhang, *InfoMat* 2019, 1, 6.
- [22] M. R. Busche, T. Drossel, T. Leichtweiss, D. A. Weber, M. Falk, M. Schneider, M.-L. Reich, H. Sommer, P. Adelhelm, J. Janek, Nat. Chem. 2016, 8, 426.
- [23] Q. Zhao, P. Chen, S. Li, X. Liu, L. A. Archer, J. Mater. Chem. A 2019, 7, 7823.
- [24] J. Wan, J. Xie, X. Kong, Z. Liu, K. Liu, F. Shi, A. Pei, H. Chen, W. Chen, J. Chen, X. Zhang, L. Zong, J. Wang, L.-Q. Chen, J. Qin, Y. Cui, Nat. Nanotechnol. 2019, 14, 705.
- [25] Q. Pan, D. M. Smith, H. Qi, S. Wang, C. Y. Li, Adv. Mater. 2015, 27, 5995.
- [26] F. N. Sayed, M.-T. F. Rodrigues, K. Kalaga, H. Gullapalli, P. M. Ajayan, ACS Appl. Mater. Interfaces 2017, 9, 43623.
- [27] K. Kanamura, T. Umegaki, S. Shiraishi, M. Ohashi, Z.-i. Takehara, J. Electrochem. Soc. 2002, 149, A185.
- [28] T. Ma, G.-L. Xu, Y. Li, L. Wang, X. He, J. Zheng, J. Liu, M. H. Engelhard, P. Zapol, L. A. Curtiss, J. Jorne, K. Amine, Z. Chen, J. Phys. Chem. Lett. 2017, 8, 1072.
- [29] P. Bai, J. Li, F. R. Brushett, M. Z. Bazant, Energy Environ. Sci. 2016,
- [30] S. Neudeck, F. Walther, T. Bergfeldt, C. Suchomski, M. Rohnke, P. Hartmann, J. Janek, T. Brezesinski, ACS Appl. Mater. Interfaces 2018, 10, 20487.
- [31] B. Li, G. Li, D. Zhang, J. Fan, D. Chen, Y. Ge, F. Lin, C. Zheng, L. Li, ChemistrySelect 2019, 4, 6354.
- [32] Q. Ran, H. Zhao, X. Shu, Y. Hu, S. Hao, Q. Shen, W. Liu, J. Liu, M. Zhang, H. Li, X. Liu, ACS Appl. Energy Mater. 2019, 2, 3120.
- [33] W. Liu, X. Li, D. Xiong, Y. Hao, J. Li, H. Kou, B. Yan, D. Li, S. Lu, A. Koo, K. Adair, X. Sun, *Nano Energy* 2018, 44, 111.
- [34] L. Liang, X. Sun, C. Wu, L. Hou, J. Sun, X. Zhang, C. Yuan, ACS Appl. Mater. Interfaces 2018, 10, 5498.

- [35] Y. Guo, H. Li, T. Zhai, Adv. Mater. 2017, 29, 1700007.
- [36] D. Zhou, R. Liu, Y.-B. He, F. Li, M. Liu, B. Li, Q.-H. Yang, Q. Cai, F. Kang, Adv. Energy Mater. 2016, 6, 1502214.
- [37] W. Fan, N.-W. Li, X. Zhang, S. Zhao, R. Cao, Y. Yin, Y. Xing, J. Wang, Y.-G. Guo, C. Li, Adv. Sci. 2018, 5, 1800559.
- [38] Q. Zhao, X. Liu, S. Stalin, K. Khan, L. A. Archer, Nat. Energy 2019, 4, 365.
- [39] L. J. Fetters, D. J. Lohse, D. Richter, T. A. Witten, A. Zirkel, *Macro-molecules*. 1994, 27, 4639.
- [40] S. Jiao, X. Ren, R. Cao, M. H. Engelhard, Y. Liu, D. Hu, D. Mei, J. Zheng, W. Zhao, Q. Li, N. Liu, B. D. Adams, C. Ma, J. Liu, J.-G. Zhang, W. Xu, Nat. Energy 2018, 3, 739.
- [41] J. Wang, Y. Yamada, K. Sodeyama, C. H. Chiang, Y. Tateyama, A. Yamada, Nat. Commun. 2016, 7, 12032.
- [42] E. Krämer, T. Schedlbauer, B. Hoffmann, L. Terborg, S. Nowak, H. J. Gores, S. Passerini, M. Winter, J. Electrochem. Soc. 2013, 160, A356.
- [43] X. Zeng, G.-L. Xu, Y. Li, X. Luo, F. Maglia, C. Bauer, S. F. Lux, O. Paschos, S.-J. Kim, P. Lamp, J. Lu, K. Amine, Z. Chen, ACS Appl. Mater. Interfaces 2016, 8, 3446.
- [44] Y. Yamada, J. Wang, S. Ko, E. Watanabe, A. Yamada, Nat. Energy 2019, 4, 269.
- [45] L. Suo, Y.-S. Hu, H. Li, M. Armand, L. Chen, Nat. Commun. 2013, 4, 1481.
- [46] L. Suo, O. Borodin, T. Gao, M. Olguin, J. Ho, X. Fan, C. Luo, C. Wang, K. Xu, Science 2015, 350, 938.
- [47] Y. Lu, Z. Tu, L. A. Archer, Nat. Mater. 2014, 13, 961.
- [48] A. Singer, M. Zhang, S. Hy, D. Cela, C. Fang, T. A. Wynn, B. Qiu, Y. Xia, Z. Liu, A. Ulvestad, N. Hua, J. Wingert, H. Liu, M. Sprung, A. V. Zozulya, E. Maxey, R. Harder, Y. S. Meng, O. G. Shpyrko, Nat. Energy 2018, 3, 641.
- [49] P. Yan, J. Zheng, J. Liu, B. Wang, X. Cheng, Y. Zhang, X. Sun, C. Wang, J.-G. Zhang, Nat. Energy 2018, 3, 600.
- [50] I. Saadoune, C. Delmas, J. Mater. Chem. 1996, 6, 193.
- [51] E. Zhao, L. Fang, M. Chen, D. Chen, Q. Huang, Z. Hu, Q.-b. Yan, M. Wu, X. Xiao, J. Mater. Chem. A 2017, 5, 1679.
- [52] Z. Liu, A. Yu, J. Y. Lee, J. Power Sources 1999, 81-82, 416.
- [53] S. H. Park, K. S. Park, Y. K. Sun, K. S. Nahm, Y. S. Lee, M. Yoshio, Electrochim. Acta 2001, 46, 1215.
- [54] T. Ohzuku, A. Ueda, M. Kouguchi, J. Electrochem. Soc. 1995, 142, 4033
- [55] S.-T. Myung, F. Maglia, K.-J. Park, C. S. Yoon, P. Lamp, S.-J. Kim, Y.-K. Sun, ACS Energy Lett. 2017, 2, 196.
- [56] H. Wang, D. Lin, Y. Liu, Y. Li, Y. Cui, Sci. Adv. 2017, 3, e1701301.
- [57] B. D. Adams, J. Zheng, X. Ren, W. Xu, J.-G. Zhang, Adv. Energy Mater. 2018, 8, 1702097.